

Supporting Information for

Changes in Supraglacial Lakes on George VI Ice Shelf, Antarctic Peninsula: 1973-2020

T. J. Barnes¹, A. A. Leeson^{1,2}, M. McMillan^{1,3,4}, V. Verjans¹, J. Carter¹ C. Kittel⁵

¹Lancaster Environment Centre, Lancaster University

²Data Science Institute, Lancaster University, Lancaster, UK

³Centre for Polar Observation and Modelling, Lancaster University, LA1 4YW, UK

⁴Centre for Excellence in Environmental Data Science, Lancaster University, LA1 4YW, UK

⁵Department of Geography, UR SPHERES, University of Liège, Belgium

Contents of this file

Text S2, S5, S6

Figure S7

Tables S3, S4

Additional Supporting Information (Files uploaded separately)

Captions for Dataset S8

Captions for Tables S1

Introduction

This supplement includes details of all satellite imagery tiles used in the study (Table S1). Elaboration of methodology, specifically method testing, is outlined in detail in Text S2. Detail regarding the selection of NDWI algorithm for this study is provided in Text S2.1, and Table S3. Additional detail on the approach taken to compensate for Landsat-7 scanline corrector failure is addressed (Text S2.2) as part of the method testing section, and also numerically justified (Table S4). Justification is given for the selection of the specific MAR climate model used in this study, with comparison to other models: RACMO2.3 and ERA5 (Text S5). Further detail covering the statistical method used in this study – the multivariate regression analysis – is provided, covering the specific backwards selection method used (Text S6).

Additional supporting findings for our study are provided, including a spatial map of the community firm model output as forced by MAR, which provides further context to our findings in regards to FAC controls on lake coverage (Figure S7). Additionally, we provide our lake polygons used in this study for download as shapefiles for use in future work (Data Set S8). This dataset may be of use to future studies of the supraglacial hydrology of GVIIS.

<Table provided as a separate document>

Table S1. Satellite images acquired for this research. Designation column refers to path and row identifiers of each tile, while full designation refers to the full tile identifier as catalogued. All tiles were used in analysis, except those listed in red, due to low study region coverage.

Text S2. Method testing detail

S2.1 NDWI Method comparison

Method testing of different NDWI methods was carried out to identify the NDWI method with the greatest efficacy for the study area. Two methods were selected for comparison: a ratio of the Blue and Red bands of satellite imagery, and a Green and Near InfraRed (NIR) method (Williamson et al., 2017). To test efficacy, we compared the results of standard NDWI lake delineation for several periods on George VI ice shelf (GVIIS) using both Sentinel-2 (S2) and Landsat-8 (LS8) images. Different months were selected to identify potential issues with solar angle, with 2019 and 2020 being used as the test years due to the high quality and frequent temporal sampling of imagery. Images were delineated and edited in line with the post-processing chain implemented in this project, removing all polygons under 1800 m², and repetitive false positives, primarily rocks. Cloud polygons were not removed here, as testing for cloud cover interference was an important part of this test. We found the Green and NIR method to be more successful on GVIIS, as there is little variance in ice shelf surface reflectance, and no blue ice, a factor the Red-Blue ratio aims to nullify. Overall, both methods were in close agreement (Table S3), with only 6% mean variance in total polygon area between each method. Maximum polygon area displayed the greatest variance due to the Red-Blue ratio being stricter on large area boundaries and the interconnectedness of lakes on GVIIS.

SATELLITE	Period	Method	Count	Total Polygon Area, m ²	Mean Polygon Area, m ²	Max Polygon Area, m ²	Min Polygon Area, m ²
Sentinel2	Jan-20	GNIR	9842	796355700	80914	245276200	1800
Sentinel2	Jan-20	RB	9916	743352600	74965	216209200	1800
Landsat8	Jan-19	GNIR	8251	680878800	82521	158217300	1800
Landsat8	Jan-19	RB	8302	611175600	73618	77863500	1800
Landsat8	Dec-19	GNIR	694	8989200	12953	856800	1800
Landsat8	Dec-19	RB	655	8890200	13573	415800	1800
Mean variance - GNIR to RB			1.42%	6.00%	4.45%	38.04%	0.00%

Table S3. Comparison of Red-Blue (RB) and Green-NIR (GNIR) NDWI methods. Minimum polygon area shows no variance due to the 2 Landsat pixel minimum value.

S2.2 Landsat 7 Correction

Due to the scanline corrector failure of Landsat-7 (LS7), output from this satellite was not initially comparable to the others due to notable data loss. To address this, we produced three sets of masking polygons of the blank areas in LS7 imagery for three different periods (January 2009, January 2007 and January 2005) in order to determine a mean data loss. We then selected several LS8 and S2 periods: January 2020, January 2018 and February 2018. The scanline data loss masks were overlain on lake polygons from these months and any obscured lakes were clipped.

Change in total lake area was calculated and averaged to find the mean total data loss, resulting in a value of 77.69% of data retained. This falls closely in line with the value provided in LS7 documentation of 78% (Ihlen & Zanter, 2019). Henceforth, we applied a conversion factor to all data not affected by the scanline failure (SLC failure), lowering their total areas by 22.31%, making all data comparable.

Period	Original Area m²	January 09	January 07	January 05
J2020 Clip	811231173	505060903 m²	732475913 m²	605258048 m²
J2020 Clip %		62.26	90.29	74.61
J2020 % Change		-37.74	-9.71	-25.39
J2018 Clip	193865900	132516651 m²	181582741 m²	147311178 m²
J2018 Clip %		68.35	93.66	75.99
J2018 % Change		-31.65	-6.34	-24.01
F2018 Clip	324645800	210647217 m²	304905648 m²	244402578 m²
F2018 Clip %		64.89	93.92	75.28
F2018 % Change		-35.11	-6.08	-24.72
Mean Clip %		65.17	92.63	75.29
Mean % Change		-34.83	-7.37	-24.71
Mean Data Loss	% Retained	% Change		
Area	77.69	-22.31		

Table S4. Output of LS7 scanline masking versus polygons in January 2020, January 2018 and February 2018. Clip and Clip % refer to the area remaining after applying the mask, while Clip % change quantifies the change from original to clipped.

Text S5. Comparison of climate models at GVIIS

Several climatic products were identified for potential use in this study: ERA5 and the regional climate models (RCMs) RACMO2.3 and MAR (Agosta et al., 2019). MAR data showed close agreement to Fossil Bluff automated weather station (AWS) recorded near-surface air temperature (SAT) values, despite MAR having the poorest spatial resolution of 35 km. MAR additionally outperformed RACMO in several winter and summer seasons during testing when comparing to the AWS data. RACMO differed on average -1.3°C from the recorded AWS values, while MAR differed by a mean of 0.6°C. ERA5 showed close agreement when corrected for lapse rate, even though it also had a relatively coarse (31 km) spatial resolution. However, ERA5 data for the 2020 melt season was not available at the time of study. RACMO2.3 showed a notable cold bias in data of 2-3°C but with a good spatial resolution of 5.5 km. Hence, MAR data was selected as it offered the most accurate and up to date values. A representative grid cell of MAR was chosen for climate simulations at centroid 71.38S, 67.83W, corresponding to the rough location of the Fossil Bluff AWS. We forced MAR with several GCM (general circulation models): CESM2, CNRM-CM6 and ACCESS1.3. These forcings were compared with MAR results when forced by ERA-Interim over 1979-2020 to evaluate their accuracy. The comparison showed good agreement (correlation coefficient = 0.8), hence providing a basis for using these forcings in future simulations to 2100. Between 1979 and 2020, MAR was forced with ERA-Interim at its boundaries. The resulting MAR data was further used to force the Community Firm Model (CFM; Stevens et al., 2020) to produce values of firn air content (FAC), refreezing, runoff and ice lens depth values.

Text S6. Regression analysis method detail

A multivariate regression was carried out including all outputs from the CFM, together with several climatic variables derived by MAR, and SAM (Marshall, 2003) in order to determine the most important controlling variables in lake coverage on GVIIS. Due to the number of variables, a backwards selection method was selected for the model. This involved the successive removal of variables from the regression model in a process of elimination. The statistic used for comparing outputs was the adjusted R^2 value rather than R^2 as adjusted R^2 penalizes regressions with large numbers of variables, thus minimizing noise fitting. Each iteration of the model involved the removal of a single non-significant ($p < 0.05$) variable judged by the individual significance value in the output. From this, variables were progressively removed until the adjusted R^2 value started to decrease upon removal of further variables. Hence, the remaining variables, the combination of which being determined as significant in impacting lake coverage, were identified as: summer total melt, November FAC, summer mean SAT, and mean annual SAM.

To identify which of these remaining variables had the greatest individual impact on lake coverage, individual regression analyses were then carried out for each variable versus lake coverage. Specifically, we carried out this analysis on summer total melt, NFAC, summer mean SAT, mean annual SAM and both summer and winter accumulation as a result of their contribution to FAC. Due to the impact of these variables on FAC, we found that FAC from the same year was less important than maintained FAC depth. Thus, accumulation was also needed for understanding the development of SGLs.

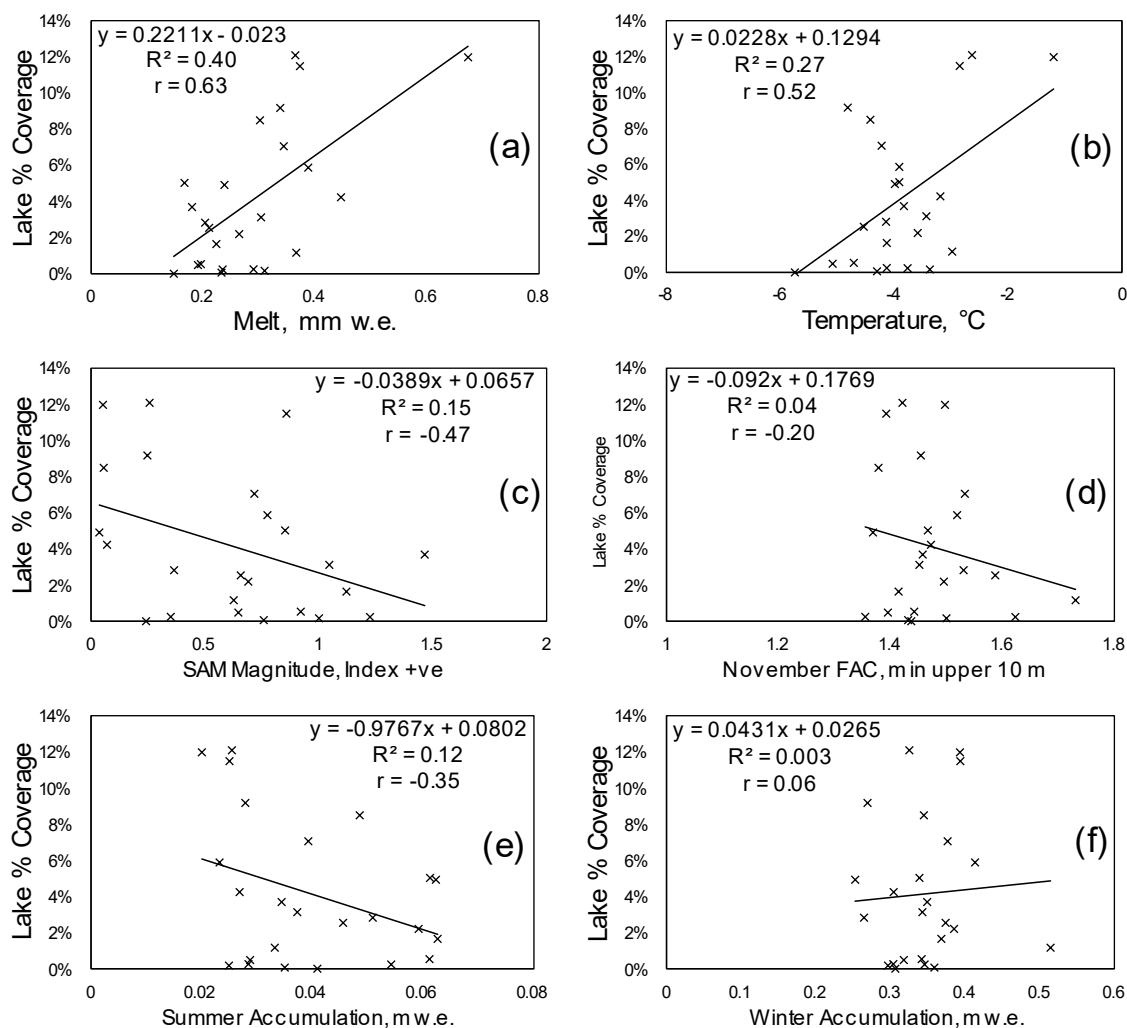


Figure S7. Scatter plots of each identified important climatic variable versus lake coverage. (a) shows melt, (b) shows temperature, (c) shows SAM magnitude, (d) shows NFAC, (e) shows summer accumulation, (f) shows winter accumulation. Temperatures were derived from the AWS data while all other variables are determined from MAR and the CFM.